Wind-wave development under alternating wind jets and wakes induced by orographic effects

Teruhisa Shimada and Hiroshi Kawamura

Ocean Environment Group, Center for Atmospheric and Oceanic Studies, Graduate School of Science, Tohoku University, Sendai, Japan

Received 15 November 2005; revised 2 December 2005; accepted 7 December 2005; published 17 January 2006.

[1] We investigate fetch-limited wind-wave development under alternating coastal wind jets and wakes induced by orographic effects. Synthetic Aperture Radar and scatterometer resolve wind jets and wakes with widths of 5–40 km. Using the wind field and a third-generation wave model, we simulate the nearshore wave field. As a result, broader directional wave spectra are seen in wakes while we can find evolution of the directional wave spectrum with offshore distance in both wind jets and wakes. Especially within the offshore distance of 40 km, directional wave spectra have two peaks. These characteristics are well reflected in the overall directional spreading field. The overall directional spreading closely corresponds to the wind speed distribution, and is small/large in wind jet/wake region. The results mean that wave energies that come from neighboring wind jet regions cross in wake regions and combine with wave energy generated by local wind in wake regions. **Citation:** Shimada, T., and H. Kawamura (2006), Wind-wave development under alternating wind jets and wakes induced by orographic effects, *Geophys. Res. Lett.*, *33*, L02602, doi:10.1029/2005GL025241.

1. Introduction

[2] A large number of studies have investigated one-dimensional fetch-limited wave growth [e.g., *Hasselmann et al.*, 1973]. The conditions have a beneficial effect on the intrinsic examination of wind-wave development. However, in most studies winds and waves are sampled along the defined fetches on the assumption that the wind is uniform in a direction transverse to the fetches all over the study area. Therefore, the discussions have been restricted only to downwind characteristics of wind-wave development.

[3] Recently, *Shimada and Kawamura* [2004] have presented alternating surface wind jets and wakes by Synthetic Aperture Radar (SAR) and scatterometer and demonstrated that in a direction transverse to the axes of the wind jets and wakes, significant wave heights (SWHs) vary along with the wind speeds. It is quite new to discuss fetch-limited wind-wave development under the two-dimensional wind configuration of alternating wind jets and wakes. We here raise questions about any modification of the wind-wave development by such a wind configuration. Standing on the case study of *Shimada and Kawamura* [2004], we investigate fetch-limited wind-wave development under alternating wind jets and wakes in terms of directional characteristics of wind waves by using a state-of-the-art wave model. In this study, wind jets and wakes are defined by relative wind speed differences.

Copyright 2006 by the American Geophysical Union.
0094-8276/06/2005GL025241$05.00

2. Data and Wave Model

[4] We carry out a pilot simulation of wind-wave development in a domain (241 $\times$ 151 pixels) with grid size of 0.01° (Figure 1). We here focus on how a wind configuration is reflected in a wave field and discuss time-independent characteristics of wave directionality. In fact, near-equilibrium wave conditions can be expected around the wind observation times [*Shimada and Kawamura*, 2004].

[5] We construct a wind field with grid size of 0.01° from the European Remote sensing Satellite (ERS) -2 SAR-derived winds. The offshore side of the model domain is covered with QuikSCAT winds at 0.25° resolution by resampling averaging their wind measurements. Despite such a simple merging way, wind jets and wakes are well reproduced continuously from nearshore to offshore. The SAR images with a nominal spatial resolution of 30 m can be converted into wind speed maps by applying SAR wind retrieval [e.g., *Scoon et al.*, 1996] using the CMOD IFR2 scatterometer model function [*Quilfen et al.*, 1998] and wind direction data used for the 6-hourly forecast of the JWA (Japan Weather Association) Local Wave Model. The typical accuracies in wind speed are 1 m/s for QuikSCAT [e.g., *Ebuchi et al.*, 2002] and about 2 m/s for SAR [e.g., *Shimada and Kawamura*, 2004]. We use wind measurements over the land at stations called Automated Meteorological Data Acquisition System (AMeDAS) operated by Japan Meteorological Agency.

[6] We use a third generation wave model SWAN (Simulating WAves Nearshore) developed for shallow waters [*Booij et al.*, 1999; *Ris et al.*, 1999]. Directional wave spectra (DWS) are computed at 180 equally spaced propagation directions (θ) and 41 logarithmically spaced frequencies (f) between $f_{\min}$ = 0.04 and $f_{\max}$ = 1.00 Hz. For main energy source terms, the following default expressions are adopted. For wind input and whitecapping, the expressions of *Komen et al.* [1984] are used. The quadruplet nonlinear wave-wave interactions are computed with the Discrete Interaction Approximation [*Hasselmann et al.*, 1985]. Bathymetric effects are not significant in this experiment. We focus on only wind-generated waves. Thus incoming waves at the open boundaries of the model domain are assumed to be zero. The SWAN model is run in stationary mode to identify an equilibrium state under the wind input. SWHs measured by ERS-2 altimeter are used to compare with the simulated SWHs.

3. Wind Field and Wind Wave Development

[7] Figure 1 shows the wind field off the Pacific coast of northern Japan on 25 February 2000 from the case study of *Shimada and Kawamura* [2004] with a focus on the present

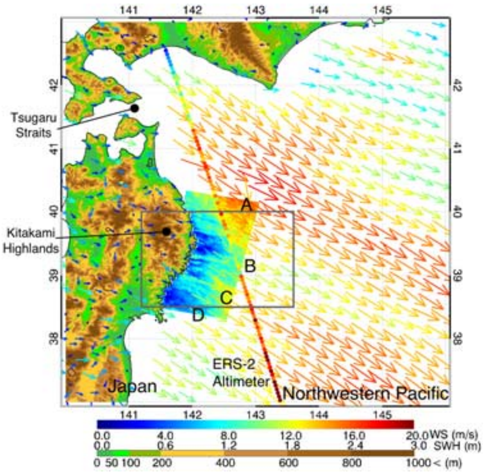

Figure 1. Ocean surface winds measured by QuikSCAT (vectors) and ERS-2 SAR (color shade). Vectors over the land are from AMeDAS. Winds are measured by QuikSCAT, ERS-2 SAR, and AMeDAS at 0906, 0115, and 0100 UT on 25 February 2000, respectively. SWHs measured by ERS-2 altimeter (1252 UT on 25 February 2000) are also plotted. The square indicates a model domain. Color scales indicate the magnitude of wind speed (WS), SWH and elevation. Geographical names are also shown. Alphabetical symbols (A–D) indicate the wind jets and wakes discussed in the text.

study area. Wind jets and wakes with typical width of 40 km are indicated in Figure 1 by the alphabetical symbols (A–D). To put it briefly, QuikSCAT wind vectors manifest two separate wind jets (A and C) with speeds above 12 m/s. They extend from the proximity of the Tsugaru Straits and the south of the Kitakami Highlands. Between these two jets, we can see a wake (B) extending downwind from the lee of the Kitakami Highlands. The SAR-derived wind map captures a part of the northern wind jet (A). Wind speeds are lower than 8 m/s in the nearshore region within 50 km from the coastline. We can see smaller-scale alternating high/low wind regions with 5–10 km widths, which correspond to indentations of the ria coast (Figure 1). We can also identify another wake (D) on the south of the wind jet (C) with wind speeds less than 6 m/s. Meanwhile, it is verified that variation of SWH along the altimeter ground track well correlated with wind speed variation. The QuikSCAT and forecast wind fields prove that wind directions are almost in the same direction over the study area and that wind convergences in the transverse direction of the axes of the wind jets and wakes are insignificant. This fact allows us to distinguish fetch-limited wind-wave development under the two-dimensional wind configuration of alternating wind jets and wakes from conventional one-dimensional fetch-limited wind-wave development.

[8] Using the wind field and SWAN, we compute the fetch-limited wind-wave development, and examine the results from the viewpoint of wave directionality (Figures 2 and 3). The model domain contains two pairs of wind jets and wakes (A–D) as shown in Figure 1. First, we investigate differences of evolution of DWS in wind jet regions and wake regions (Figure 2). We define two lines in the wind jet (C) and wake (B) along the wind direction, i.e. fetch, as shown in Figure 4a, and choose representative grid points with offshore distances of 20, 40, and 70 km for each line. Polar plots in Figure 2 represent the DWS together with the local wind directions at the grid points.

[9] Figures 2a–2c show the evolution of DWS in the wind jet regions with the offshore distance. With increasing offshore distance, the peak energy increases and the peak frequency downshifts. They all have one primary spectrum peak, and the spectral shapes do not change significantly with the offshore distance. The directions of the spectrum peaks coincide with local wind directions all over the offshore distances. The above-mentioned characteristics are typical aspects of one-dimensional fetch-limited wind wave growth. On the other hand, the DWS in the wake region show different spectrum evolution (Figures 2d–2f). The spectrum energy evolves with the offshore distance, but they are lower than those in the wind jet region. The spreading of DWS at lower frequencies is much broader than those in the wind jet region. In particular, bimodal DWS are shown at the distance of 20 and 40 km. The directions of the two peaks are 30° and 260°, deviating more than 40° from the local wind direction. At the distance of 70 km, the DWS (Figure 2f) is unimodal and the spectrum shape is similar to the DWS in the wind jet region (Figure 2c).

[10] We can comprehensively examine the differences of spectrum directionality between wind jet regions and wake regions by taking notice of the overall directional spreading (DSPR) field. The overall DSPR can be considered as a weighted average of the DSPR (the one-sided directional width of the spectrum) per frequency, and defined as [*Kuik et al.*, 1988]:

$$DSPR^2 = \left(\frac{180}{\pi}\right)^2 \cdot \left[2 - 2\frac{\left\{ \left(\int_{f_{\min}}^{f_{\max}} \int_0^{2\pi} \cos\theta E(f,\theta) d\theta df \right)^2 + \left(\int_{f_{\min}}^{f_{\max}} \int_0^{2\pi} \sin\theta E(f,\theta) d\theta df \right)^2 \right\}^{1/2}}{\int_{f_{\min}}^{f_{\max}} \int_0^{2\pi} E(f,\theta) d\theta df} \right], \quad (1)$$

where $E(f, \theta)$ is DWS.

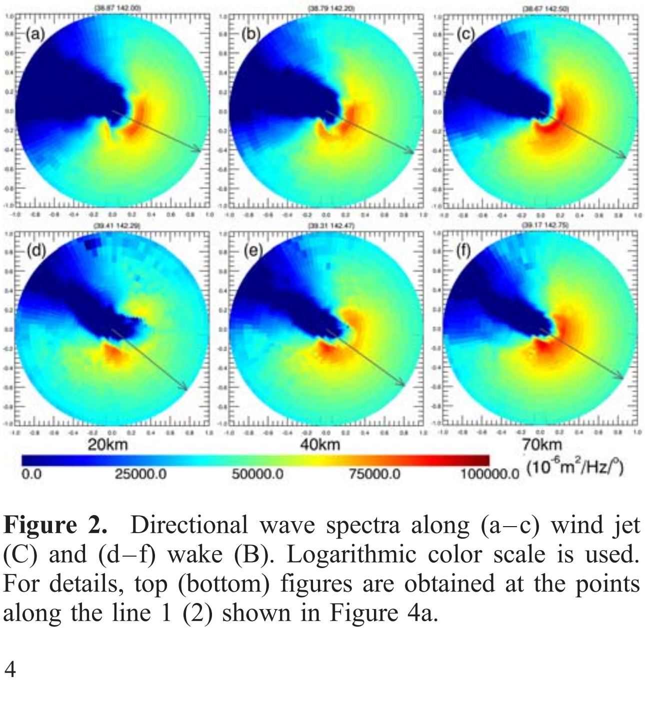

Figure 2. Directional wave spectra along (a–c) wind jet (C) and (d–f) wake (B). Logarithmic color scale is used. For details, top (bottom) figures are obtained at the points along the line 1 (2) shown in Figure 4a.

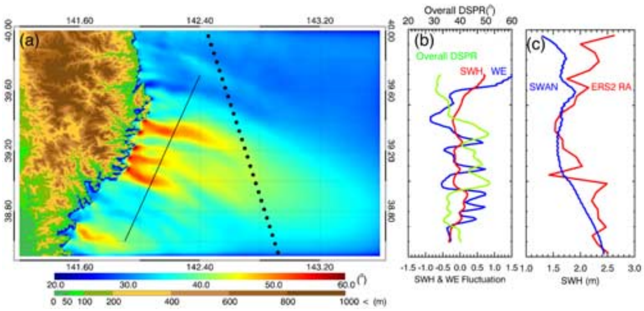

Figure 3. (a) Overall DSPR field. (b) SWH fluctuation (red), wind energy (WE) fluctuation (blue) and the overall DSPR (green) are plotted along the solid line in Figure 3a. (c) Comparison between the simulated and altimeter observed SWHs along the altimeter ground track indicated by the dotted line in Figure 3a.

[11] The effects of alternating wind jets and wakes are remarkably reflected in the overall DSPR field (Figure 3). To put it into perspective, we can find that the regions of the wind jets (A and C) correspond to lower overall DSPR (<30° for A and <40° for C) and the regions of the wakes (B and D) correspond to higher overall DSPR (>40° for B and D). Then, we take a close look at smaller-scale wind variations in the nearshore region (Figure 4a). We can also see the same relation between wind speed and the overall DSPR (Figure 4b). Namely, the overall DSPR is large (>50°) in the nearshore wake regions and small (<45°) in the nearshore wind jet regions. These patterns well correspond to indentations of the ria coast (Figure 4).

[12] Figure 3b shows variation of wind energy (square of wind speed), the overall DSPR, and the computed SWH along the solid line indicated in Figure 3a. The line intersects the axes of the nearshore wind jets and wakes. For intercomparison of their fluctuations, the following parameter is defined as:

$$\delta I/I_0 = (I - I_0)/I_0, \qquad (2)$$

where I is wind energy and SWH along the line and I_0 is average over the line. SWH variation coincides with wind energy variation. However, the SWH fluctuations are much smaller than those of wind energy. On the other hand, it is also ascertainable from Figure 3b that the overall DSPR is negatively correlated with wind energy.

[13] The computed SWHs are compared with SWHs from ERS-2 altimeter along the ground track (Figure 3c). It can be concluded that SWH variations are generally well reproduced by SWAN. This result supports the reasonableness of the simulation with a focus on nearshore regions. At higher latitudes (>39.7°N), SWHs are underestimated because the model domain does not completely contain the wind jet (A) or because incoming wave energy is assumed to be zero. However, the fact has no relation to the essence of the study.

4. Discussion

[14] From the results above, we can propose a conceptual model for the different directionalities of DWS in wind jet regions and wake regions as below. One wind jet/wake promotes the formation of relatively weak/strong wind on both sides, inducing a configuration of alternating wind jets and wakes. Wind waves are generated and developed downwind by local wind both in regions of wind jets and wakes. More energy is transferred to wind waves from local wind in wind jet regions than in wake regions. On the other hand, in all wind conditions, wave components propagate at a range of angles beyond the range of variation of local wind direction. This directional spreading, associated with wave energy transfer processes, is frequency dependent [e.g., *Young et al.*, 1995]. However, energies that spread from wind jet regions are much larger than those from wake regions. Thus, the dominant wave energies outflowing from wind jet regions cross each other in neighboring wake regions, and combine with wave energy developed by local wind in wake regions. That is to say, wave energies incoming from neighboring wind jet regions induce broader DWS in wake regions. In cases where the wind speed contrast between wind jets and wakes is large, bimodal DWS are seen in wake regions. Departing at a certain distance from the coast, higher spectrum energy aligns along the local wind direction, and bimodal peaks in the DWS disappear. This is because the wind speed contrast between wind jets and wakes decreases with offshore distance and because wave spectrum energy in wake regions grows in equal measure with spectrum energy inflowing from the neighboring wind jet regions. Such directional characteristics of wind waves are not reflected in the computed SWH field because SWH is an integrated parameter of wave spectrum over the direction. This conceptual model casts the orographic modification of wind as the ultimate cause of the directionality of wave spectra in coastal seas. Observational studies are required to make sure of the sequence of the processes. Further studies are required to investigate the dependence of spectrum width on characteristics of wind fields such as wind speeds, wind speed differences between wind jets and wakes, widths of wind jets and wakes and time variation.

[15] In the case of addressing fetch-limited wave growth in deep water, the following source terms in the action balance equation of SWAN can play a significant role in directional spreading: the generation by wind, dissipation by whitecapping, and nonlinear wave-wave interactions. Because high-frequency wave components respond relatively quickly to wind direction [e.g., *van Vledder and Holthuijsen*, 1993], wind variability is successful in generating broader DWS [*Ponce and Ocampo-Torres*, 1998]. Directional distri-

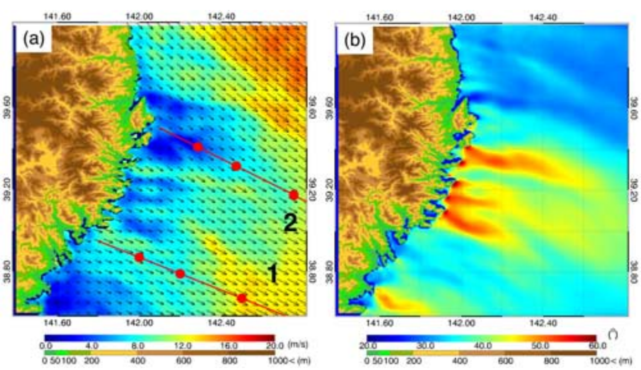

Figure 4. Close-up views of (a) the wind field and (b) the overall DSPR with a focus on the nearshore region. As to the two red lines in Figure 4a, see the caption of Figure 2.

bution functions incorporated in wind input source term are conducive to broader DWS (e.g., the first power of cosine by *Komen et al.* [1984]). A reduced directional spreading has been observed when dissipation is relatively high [*Banner and Young*, 1994]. Above all, many studies stress that nonlinear wave-wave interactions dominantly induce spreading of the wave directional structure [e.g., *Young and van Vledder*, 1993]. In the present case, the input wind energy distribution is complex due to the wind speed differences between wind jets and wakes. Wave energy imbalance induced by such wind input should be compensated by the nonlinear wave-wave interactions. Consequentially, spectrum shapes in wake regions come close to those in wind jet regions with offshore distance. It remains as a future challenge to examine the directional distributions of the source terms, and their balance. To consider these points, full representation of nonlinear wave-wave interactions should be adopted [e.g., *Young et al.*, 1995].

5. Summary and Concluding Remarks

[16] We simulate wind-wave development under alternating wind jets and wakes with typical widths of 5–40 km by using SWAN wave model and the high-resolution wind field resolved by SAR and scatterometer. The following conclusions are obtained.

[17] 1. Broader directional wave spectra are seen in the wake region than those in the wind jet region. Moreover, bimodal directional wave spectra are distinguished with offshore distances of less than 40 km. The directions of the two peaks are at angles of more than 40° from the local wind direction.

[18] 2. The spatial distribution of the overall directional spreading corresponds to the wind speed variation associated with the wind jets and wakes. The overall directional spreading is large in the wake regions and small in the wind jet regions.

[19] This study demonstrates that wind configuration of alternating wind jets and wakes has a great impact not only on difference of wind energy input but also on energy transfer between waves. Namely, such a wind configuration induces different directionality in wave field. This study can be also characterized as a counterpart of the swell sheltering effect of islands, inducing complex spectrum directionality in the lee of the islands [*Ponce de Leòn and Guedes Soares*, 2005]. The characteristic directionality of ocean surface wave fields brings better understanding of high individual wave occurrences, spectrum shapes, sea surface slopes, and wave energy transfer.

[20] **Acknowledgments.** ERS-2 SAR data were provided from Japan Aerospace Exploration Agency. QuikSCAT data were obtained from NASA Physical Oceanography Distributed Active Archive Center at the Jet Propulsion Laboratory. AMeDAS data were provided by the Japan Meteorological Agency. The authors thank the SWAN team for making SWAN available. Outputs of Local Wave Forecast Model are purchased from Japan Weather Association. Bathymetric data from Japan Oceanographic Data Center were used for wave simulation. The SWAN simulations are carried out using the supercomputer system SX-7 of Information Synergy Center, Tohoku University. We thank two anonymous reviewers for their careful reading of the manuscript and constructive suggestions for improvement.

References

Banner, M. L., and I. R. Young (1994), Modeling spectral dissipation in the evolution of wind waves: Part I. Assessment of existing model performance, *J. Phys. Oceanogr.*, *24*, 1550–1571.

Booij, N., R. C. Ris, and L. H. Holthuijsen (1999), A third-generation wave model for coastal regions: 1. Model description and validation, *J. Geophys. Res.*, *104*, 7649–7666.

Ebuchi, N., H. C. Graber, and M. J. Caruso (2002), Evaluation of wind vectors observed by QuikSCAT/SeaWinds using ocean buoy data, *J. Atmos. Oceanic Technol.*, *19*, 2049–2062.

Hasselmann, K., et al. (1973), Measurement of wind-wave growth and swell decay during the Joing North Sea Wave Project (JONSWAP), *Dtsch. Hydrogr. Z.*, *8*(12), Suppl. A, 95.

Hasselmann, S., K. Hasselmann, J. H. Allender, and T. P. Barnett (1985), Computations and parameterizations of the nonlinear energy transfer in a gravity-wave spectrum: Part II. Parameterization of the nonlinear energy transfer for application in wave models, *J. Phys. Oceanogr.*, *15*, 1378–1391.

Komen, G. J., S. Hasselmann, and K. Hasselmann (1984), On the existence of a fully developed wind-sea spectrum, *J. Phys. Oceanogr.*, *14*, 1271–1285.

Kuik, A. J., G. P. van Vledder, and L. H. Holthuijsen (1988), A method for the routine analysis of pitch-and-roll buoy wave data, *J. Phys. Oceanogr.*, *18*, 1020–1034.

Ponce, S., and F. J. Ocampo-Torres (1998), Sensitivity of a wave model to wind variability, *J. Geophys. Res.*, *103*, 3179–3201.

Ponce de Leòn, S., and C. Guedes Soares (2005), On the sheltering effect of islands in ocean wave models, *J. Geophys. Res.*, *110*, C09020, doi:10.1029/2004JC002682.

Quilfen, Y., B. Chapron, T. Elfouhaily, K. Katsaros, and J. Tournadre (1998), Observation of tropical cyclones by high-resolution scatterometry, *J. Geophys. Res.*, *103*, 7767–7786.

Ris, R. C., N. Booij, and L. H. Holthuijsen (1999), A third-generation wave model for coastal regions: II. Verification, *J. Geophys. Res.*, *104*, 7667–7681.

Scoon, A., I. S. Robinson, and P. J. Meadow (1996), Demonstration of an improved calibration scheme for ERS-1 SAR imagery using scatterometer wind model, *Int. J. Remote Sens.*, *17*(2), 413–418.

Shimada, T., and H. Kawamura (2004), Wind jets and wind waves off the Pacific coast of northern Japan under winter monsoon captured by combined use of scatterometer, SAR and altimeter, *J. Geophys. Res.*, *109*, C12027, doi:10.1029/2004JC002450.

van Vledder, G. P., and L. H. Holthuijsen (1993), The directional response of ocean waves to turning winds, *J. Phys. Oceanogr.*, *23*, 177–192.

Young, I. R., and G. P. van Vledder (1993), A review of the central role of the nonlinear interactions in wind-wave evolution, *Philos. Trans. R. Soc. London, Ser. A*, *342*, 505–524.

Young, I. R., L. A. Verhagen, and M. L. Banner (1995), A note on the bi-modal directional spreading of fetch-limited wind waves, *J. Geophys. Res.*, *100*, 773–778.

H. Kawamura and T. Shimada, Ocean Environment Group, Center for Atmospheric and Oceanic Studies, Graduate School of Science, Tohoku University, Aramaki Aza Aoba, Aoba-ku, Sendai, Miyagi, Japan 980-8578. (shimada@ocean.caos.tohoku.ac.jp)